I&EC research
Industrial & Engineering Chemistry Research

Article

Cite This: Ind. Eng. Chem. Res. 2019, 58, 13274−13283

pubs.acs.org/IECR

Tuning *n*-Alkane Adsorption on Mixed-Linker Zeolitic Imidazolate Framework-8-90 via Controllable Ligand Hybridization: Insight into the Confinement from an Energetics Perspective

Hui Sun,[*,†,‡] Hao Jiang,[‡] Ruiqi Kong,[‡] Danni Ren,[‡] Dan Wang,[‡] Jialun Tan,[‡] Di Wu,[§,∥,⊥,#] Weinan Zhu,[‡] and Benxian Shen[†,‡]

[†]International Joint Research Center of Green Energy Chemical Engineering, East China University of Science and Technology, Shanghai 200237, China

[‡]Petroleum Processing Research Center, East China University of Science and Technology, Shanghai 200237, China

[§]Alexandra Navrotsky Institute for Experimental Thermodynamics, Washington State University, Pullman, Washington 99163, United States

[∥]The Gene and Linda Voiland School of Chemical Engineering and Bioengineering, Washington State University, Pullman, Washington 99163, United States

[⊥]Materials Science and Engineering, Washington State University, Pullman, Washington 99163, United States

[#]Department of Chemistry, Washington State University, Pullman, Washington 99163, United States

Supporting Information

ABSTRACT: Linker hybridization provides enormous tunability of structures and properties of zeolitic imidazolate frameworks (ZIFs). We synthesized hybrid ZIF-8-90 structures by using binary organic ligands and examined their compositional and structural evolution using multiple techniques including field emission scanning electron microscopy (FESEM), Raman, X-ray diffraction (XRD), thermogravimetry-differential scanning calorimetry (TG-DSC), N_2 adsorption, and ^1H NMR analyses. Well-designed ligand compositions of ZIF structures contribute to the continuously switchable pore structures. The average micropore diameter shrinks from 0.72 to 0.65 nm, while the mesopore width monotonically increases from 2.18 to 3.29 nm as the carboxaldehyde-2-imidazole (OHC-IM) proportion rises from 0.31 for ZIF-8-90-S1 to 0.88 for ZIF-8-90-S5. An increase in framework polarity can lead to the strengthened guest−host interaction and therefore energetically exerts a positive effect on the adsorption affinity of *n*-hexane on hybrid ZIF-8-90 structures. The highest *n*-hexane adsorption capacity is found on the ZIF-8-90-S4 sample (having OHC-IM proportion of 0.82). At a close OHC-IM proportion of 0.792, the simulation result exhibits the strongest guest−host interaction (with the largest van der Waals interaction energy).

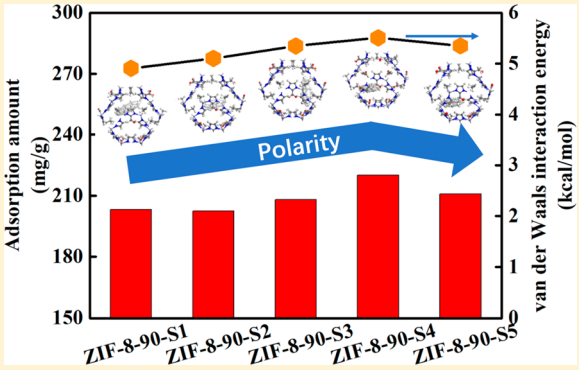

1. INTRODUCTION

The chemical industry usually needs to carry out effective separation of hydrocarbon mixtures including normal/isomeric alkanes,[1] alkanes/alkenes,[2,3] and aromatic isomers[4] in order to ensure high-valued utilization of individual components contained in mixtures or upgrade product quality by removing impurities. Normal alkanes (*n*-alkanes) are usually separated from hydrocarbon mixtures to increase octane number of gasoline distillates,[5] improve cryogenic performance of liquid fuels,[6] and feed the production of a series of petrochemicals, including alkyl benzene, sodium benzoate, lubricating oil additives, and so on.

At present, a variety of methods have been reported to separate *n*-alkanes from various isomers. Bury et al.[7] focused on an diamondoid NPM-based oxidotetrazinc cluster (named DiaMM-1) and found that DiaMM-1 could exhibit a high adsorbate diffusivity as well as low adsorption energy and, therefore, lead to high-efficiency separation of hexane isomers at low temperature. Espada et al.[8] conducted the extraction of waxes from different crude oils by using the sequential chromatographic method. Besides, distillation,[9] membrane separation,[10,11] and the urea-adduct process[12] have also been reported to apply for *n*-alkanes separation. Among these processes, adsorption has the advantages of low energy consumption,[7] high selectivity,[13] and good product purity.[14]

Received: February 18, 2019
Revised: June 15, 2019
Accepted: June 27, 2019
Published: June 27, 2019

DOI: 10.1021/acs.iecr.9b00941
Ind. Eng. Chem. Res. 2019, 58, 13274−13283

Therefore, adsorption has been receiving extensive attention from the academic and industrial fields.

A variety of adsorbents including several types of molecular sieve,[15−17] a number of metal−organic frameworks (MOFs),[18−20] porous organic polymer materials,[21,22] and functionalized metal oxides[23,24] have been widely used for the separation of linear alkanes from hydrocarbons. Among these porous materials, MOFs are known as nanoporous structures consisting of changeable metal centers bound to each other via diverse organic ligands.[25,26] In recent years, they have gained considerable attention in a wide research field involving adsorption, separation, catalysis, energy storage, electronics, sensors, and medicine,[27−32] owing to their changeable metal sites as well as tunable pore structure and continue to intrigue due to the rational synthesis of a plethora of intricate framework topologies.

Specifically, zeolitic imidazolate frameworks (ZIFs), one group of frameworks having structural topologies equivalent to zeolites (through replacing tetrahedral Si and Al in zeolites with transition metals (e.g., Zn or Co) and the bridging O atoms with imidazolate linkers), have drawn much attention and been synthesized using a variety of methods.[33−38] Synthetic ZIF materials with different voids and channels can be used to host diverse guest molecules and offer large flexibility in function modification. In addition, as compared to most other MOFs, ZIFs are proven to exhibit better thermal, hydrothermal, and chemical durabilities, which partially leads to increasing research interests in adjustment of physical and chemical features in order to attain satisfactory performances in a wide range of potential applications.[39−41] Hupp et al.[42] improved hydrogen storage capacity by 86% via loading Li ions on a double-perforated material of $Zn_2(NDC)_2(diPyNI)$ (NDC = 2,6-dicarboxylate, diPyNI = *N*,*N*′-di(4-pyridyl)-1,4,5,8-naphthalenetetracarboxydiimide) which contains oxidizing active ligand. Eum et al.[43] successfully synthesized a series of ZIF-8-90 structures and highlighted their tunable molecular sieving for linear and branched alkane molecules in terms of kinetic diffusion. The diffusivities could be changed largely through modifying the pore window sizes, and the *n*-butane adsorption selectivity over *i*-butane was revealed from the diffusion kinetics perspective. Beyond that, the confinement of hydrocarbon molecules in pore-regulated nanoporous ZIF structures and the guest−host interactions relating to both chemical and structural properties are fundamentally important and play crucial roles in determining the tunable adsorption selectivity of normal alkanes over isomeric ones.

In the present work, hybrid ZIF-8-90 structures were synthesized and used for the *n*-alkane selective adsorption over *i*-alkane, which is an adsorption of enormous importance for the chemical industry. A series of mixed-linker ZIF-8-90 samples were successfully prepared via hybridizing organic ligands of 2-methylimidazole (2-MeIM, linker of ZIF-8) and carboxaldehyde-2-imidazole (OHC-IM, linker of ZIF-90) into the metal−organic frameworks and characterized using multiple techniques. Adsorption measurements coupled with GCMC simulation were carried out to evaluate the tunable *n*-hexane adsorption performances of hybrid ZIF-8-90 samples. Here we correlate the structural evolution with capturing affinity to probe molecule and highlight the tunability of adsorption properties from the energetics prospective.

2. MATERIALS AND METHODS

2.1. Materials. Sodium formate (HCOONa) (with >99% purity), 2-MeIM (with >98% purity), and $Zn(NO_3)_2{\cdot}6H_2O$ (with >99% purity) were purchased from Shanghai Macklin Biochemical Co., Ltd. (Shanghai, China). Methanol (MeOH) and carboxaldehyde-2-imidazole (with >98% purity) were obtained from Meryer Chemical Technology Co., Ltd. (Shanghai, China). Deionized H_2O was used in all cases. All the chemicals were used without further purification.

2.2. Synthesis of ZIF-8 and ZIF-90. ZIF-8 and ZIF-90 were synthesized according to the previously reported method.[44] In ZIF-8 synthesis, 20 mmol of 2-MeIM and 40 mmol of HCOONa were dissolved in 200 mL of MeOH under magnetic stirring. A volume of 200 mL of MeOH solution with 100 mmol of $Zn(NO_3)_2{\cdot}6H_2O$ was added to the previous solution. The reaction mixture then was transferred to a Teflon-lined stainless steel autoclave and maintained at 363 K for 18 h. Hereafter, the resulting mixture was cooled and the ZIF-8 product was separated by centrifugation, washed with MeOH thrice, and dried at 333 K for 12 h.

For ZIF-90 synthesis, 40 mmol of OHC-IM and 10 mmol of $Zn(NO_3)_2{\cdot}6H_2O$ were dissolved into 100 mL of DMF in a glass jar under stirring. The solution was heated at 393 K while stirring for 10 min. The resulting light-orange solution was kept at room temperature for 24 h. The ZIF-90 product was separated from the reaction solution by centrifugation, washed with MeOH thrice, and dried at 353 K for 12 h.

2.3. Synthesis of ZIF-8-90. Five ZIF-8-90 samples were synthesized following a procedure previously reported[45] but a slightly modified crystallization procedure. By introducing a nonsolvent media, a drastic solubility change in the reaction solution occurs and rapid crystallization will happen. As a result, there will be a significant reduction in the induction period that involves precursor formation and nucleation. In order to synthesize hybrid ZIF-8-90 frameworks, 20 mmol of HCOONa, x mmol of OHC-IM (x = 5, 7.5, 10, 12.5 and 15), and $(20 - x)$ mmol of 2-MeIM were dissolved in 50 mL of MeOH to obtain a series of mixed-linker reaction solution I with x varying from 0 to 20. Solution II was prepared via dissolving 5 mmol of $Zn(NO_3)_2{\cdot}6H_2O$ into 50 mL of deionized H_2O. The Zn salt solution II was mixed with the IM solution I at room temperature and continued to stir for 1 h. The resulting mixtures were centrifuged for 10 min to collect the solid products. The samples were washed three times with MeOH and dried at 358 K for 12 h. The resulting five samples were labeled as ZIF-8-90-S1, ZIF-8-90-S2, ZIF-8-90-S3, ZIF-8-90-S4, and ZIF-8-90-S5, respectively (see Table 2).

2.4. Simulation Details. All simulations were carried out using a Materials Studio 7.0 package (Accelrys Ltd.). The adsorption isotherms of *n*-hexane on various ZIF structures were calculated by using the Grand Canonical Monte Carlo (GCMC) method and the configurational bias method with periodic boundary conditions implemented in the Accelrys Sorption module.[46]

The starting ZIF-8 (structure code VELVOY[47]) and ZIF-90 (structure code WOJGEI[48]) unit cells were obtained from the Cambridge Structural Database (CSD)[49] and depicted in Figure 1. According to compositions of organic ligands in ZIF-8-90 structures determined by ^{1}H NMR analysis, we randomly distributed the two linker ligands to produce a series of ZIF-8-90 frameworks having the OHC-IM to 2-MeIM molar ratios of 1:2, 1:1, 2:1, 19:5, and 7:1, basically consistent with

DOI: 10.1021/acs.iecr.9b00941
Ind. Eng. Chem. Res. 2019, 58, 13274−13283

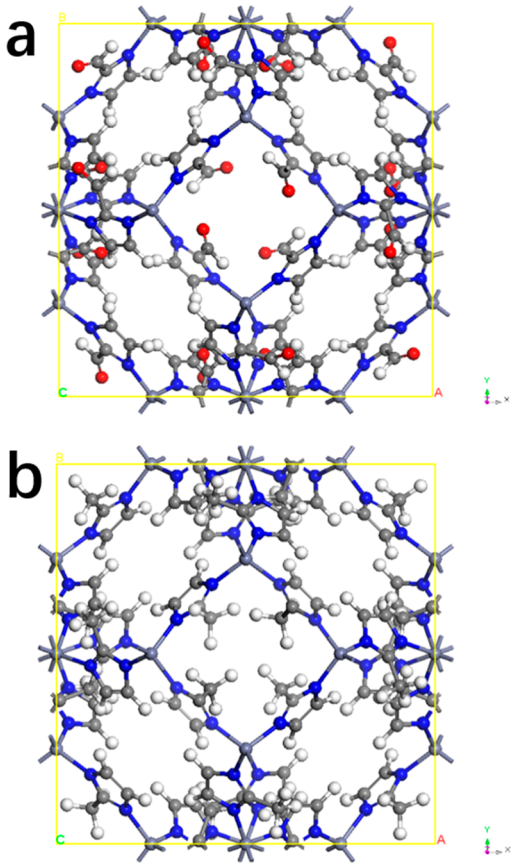

Figure 1. Unit cell structures of (a) ZIF-90 and (b) ZIF-8 viewed along the (0,0,1) direction.

experimentally observed values. The original structures contain oxygen atoms bonded to zinc centers. These oxygen atoms were removed from the frameworks in our simulation to represent the dehydrated structures. A 2 × 2 × 2 unit cell of the ZIF-8-90 was used in our simulation, and the charge of atoms in the framework was assigned according to the connectivity-based atom contribution (CBAC)[50] method. The Cartesian and fractional atomic positions were fixed to restrict the adsorption simulation in a specific region.

The *n*-hexane module was established using a united-atom description, considering each CH_2/CH_3 group as a single interaction center with effective potential parameters. Applying this approach, *n*-hexane is composed of two $CH_3(sp^3)$ and four $CH_2(sp^3)$ groups.[51,52] Each guest site is electronically neutral and interacts with other adsorbate molecules and/or host framework sites via a Lennard–Jones 12-6 potential.[53,54] Parameters for *n*-hexane sites were derived from the work of Dubbeldam et al.[55] These parameters result from a reparameterization of the standard TraPPE-UA force field commonly used in adsorption simulation studies.[56,57]

Lennard–Jones potential parameters for ZIF-8-90 frameworks were obtained using the DREIDING force field.[58] These parameters were proven to give consistent simulation results to experimental adsorption data of *n*-hexane in MOFs.[59] In the simulation, all bond lengths were considered to be rigid, while bond angles were allowed to bend. Table 1 lists the Lennard–Jones potential parameters used in this study. Interactions between different sites were computed according to the standard Lorentz–Berthelot combining rule, and all interactions were cut off at a distance of 13 Å and a cubic spline

Table 1. Lennard–Jones Potential Parameters for Adsorbate Groups and ZIF Framework Atoms

site	σ^a (Å)	$\varepsilon/k_B{}^b$ (K)
CH_3 (sp^3)	3.760	108.00
CH_2 (sp^3)	3.960	56.00
Zn	4.540	27.68
N	3.662	38.95
O	3.033	48.16
C	3.476	47.86
H	2.846	7.650

[a]σ = size parameter. [b]ε and k_B = strength parameter and Boltzmann constant.

truncation of width of 1 Å. The Ewald summation method was used to handle the electrostatic interactions between guest and host atoms with an accuracy of 0.001 kcal/mol. The guest–host potential energies and the density field of the guest molecules were sampled by 25 points between two evaluations of the field data on a three-dimensional grid of 0.25 Å grid spacing.

Adsorption isotherms and van der Waals interaction energy were calculated by GCMC simulation, in which the temperature (T), volume (V), and chemical potential (μ) of the system were kept fixed, while the system energy (E), pressure (P), and total number of molecules (N) fluctuate. For each isotherm point, the computational process was equilibrated during 5 000 000 steps and followed by 5 000 000 production steps for data collection. In order to compare the simulated isotherms to experimental results, the predicated data were converted from absolute values to excess adsorption amounts.

2.5. Characterizations. Pore structures of different samples were determined by N_2 adsorption at 77 K using a 3H-2000PM2 automatic physisorption analyzer (BeiShiDe Instrument Co., Ltd., Beijing, China). All samples were outgassed at 423 K under vacuum for 6 h prior to measurements. The specific surface area was calculated using the Brunauer–Emmett–Teller (BET) method. Micropore and mesopore volumes were calculated using the Harvath–Kawazoe (H–K) method and the Barrett–Joyner–Halenda (BJH) method, respectively. Powder X-ray diffraction (XRD) analyses on synthetic samples were carried out on a Rigaku D/max 2550 diffractometer (Rigaku Industrial Corporation, Japan) using Cu Kα (λ = 1.5418 Å) as an X-ray source. The patterns were collected over a 2θ range from 5° to 75° with a scanning speed of 5 deg/min. The crystal sizes and morphological features of ZIF samples were determined by means of field emission scanning electron microscopy (FESEM) conducted on a NOVA Nano SEM450 microscope (FEI) operated at a beam current of 10 nA and accelerating voltage of 15 kV. Raman spectra were collected by using a Renishaw InVia Reflex Raman spectrometer (Renishaw Plc., U.K.) equipped with a 785 nm argon ion laser. Data were recorded from 4000 to 100 cm^{-1} with a spectral resolution of 1.14 cm^{-1} and using a grating of 2400 lines/mm. Thermogravimetry and differential scanning calorimetry (TG-DSC) analyses were conducted on a SDTQ600 system (TA Instruments). Samples were placed in a platinum crucible and heated from room temperature to 800 °C at 10 °C/min under 100 mL/min oxygen flow. ^1H NMR measurements were performed using an Avance III 400 MHz spectrometer after digesting the ZIF samples in d_4-acetic acid (CD_3CO_2D). The chemical shifts of both imidazole linkers (OHC-IM and 2-

DOI: 10.1021/acs.iecr.9b00941
Ind. Eng. Chem. Res. 2019, 58, 13274–13283

MeIM) were referenced to CD_3CO_2D (chemical shift of 2.04 ppm). In order to confirm the composition of the two imidazole linkers in the hybrid ZIF-8-90 structures, the integrated peak areas of the methyl protons of 2-MeIM (2.65 ppm) and the aldehyde proton of OHC-IM (9.84 ppm) were calculated (see ^{1}H NMR spectra in Figure S1).

2.6. Liquid Phase Adsorption. The adsorption performance of ZIF samples with different ligand compositions were evaluated by the uptakes of *n*-hexane from a *n*-hexane/cyclohexane binary solution. In total, 0.3 g of ZIF sample was immersed into a glass vessel containing 4.5 g of binary solution with a *n*-hexane mass fraction of 5%. All static adsorption experiments were carried out at 298 K. The equilibrated concentrations of *n*-hexane in solution were determined by using a GC-920 gas chromatograph (Shanghai Huaai Chromatography Analysis Co., Ltd., Shanghai, China) equipped with a flame ionization detector and capillary column (50 m × 0.2 mm). The adsorption capacities for *n*-hexane, *Q* (mg of *n*-hexane per g of adsorbent), can be simply calculated from the initial and equilibrated concentrations of *n*-hexane in the liquid phase according to eq 1.

$$Q = \frac{m_l(c_0 - c)}{m_s} \times 10^3 \quad (1)$$

where m_l and m_s are the masses of the binary solution and adsorbent sample (g), respectively. c_0 and c are the initial and equilibrated mass fractions of *n*-hexane in the solution (%), respectively.

2.7. Gas Phase Adsorption. Gas phase adsorption isotherms of *n*-hexane on different ZIF samples were determined at 298 K using a 3H-2000PW gravimetric vapor adsorption analyzer (BeiShiDe Instrument Co., Ltd., Beijing, China). All samples were degassed at 423 K under vacuum for 6 h prior to measurements. The adsorption data at each pressure point were obtained until the samples reached adsorption equilibrium.

3. RESULTS AND DISCUSSION

3.1. Ligand Composition Analyses. We did Raman spectroscopy analyses in order to confirm the molecular structures of the synthesized ZIF samples (see Figure 2). In the spectrum of each ZIF sample, the wavenumber range of 2000 to 600 cm^{-1} is associated with the organic groups of the metal−organic frameworks. Specifically, absorption peaks at 1470 and 1670 cm^{-1} correspond to the in-plane antisymmetry vibration of the methyl group in the 2-MeIM ligand and the stretching vibration of the aldehyde group contained in the OHC-IM ligand, respectively. They can be considered as the characteristic absorption peaks of the ZIF-8 and ZIF-90 linkers, respectively. In addition, the two organic ligands can be further distinguished from the spectra focused on the wavenumber range of 1100−1500 cm^{-1}. For the ZIF-8 sample, the spectrum shows four absorption events appearing at 1500 cm^{-1} (C═N stretching vibration), 1380 cm^{-1}(−CH_3 symmetry deformation vibration), and 1180 and 1150 cm^{-1} (−CH in-plane bending vibration of imidazole). As for the ZIF-90 sample, the spectrum exhibits shifting wave numbers at 1420 cm^{-1} (C═N stretching vibration), 1360 cm^{-1} (H−C stretching vibration of aldehyde group), 1320 cm^{-1} (C−H wagging vibration of aldehyde group), and 1200 and 1130 cm^{-1} (−CH in-plane bending vibration of imidazole). In the case of ZIF-8-90 samples, all absorption peaks appearing in spectra of ZIF-8 and ZIF-90 can be observed, indicating that mixed-linker ZIF-8-90 structures were successfully synthesized.[60] However, the possibility of the presence of ZIF-8 and ZIF-90 crystal mixtures in ZIF-8-90 samples cannot be excluded.

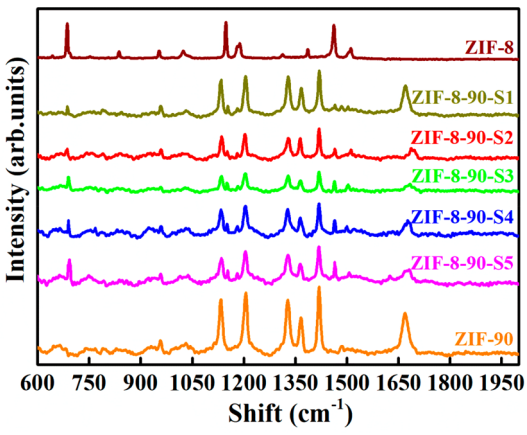

Figure 2. Raman spectra of different samples.

To figure out the average ligand compositions in five synthesized ZIF-8-90 samples, liquid phase ^{1}H NMR spectroscopy analyses were carried out (see Figure S1 for the ^{1}H NMR spectra and Table 2 for the compositions of the OHC-IM and 2-MeIM ligands). Ligand compositions in the crystallized materials are found not identical to that originally contained in the synthesis solutions because of the distinct difference of solubility as well as bonding affinity between two kinds of ligand. In addition, the possible presence of crystal mixtures of ZIF-8 and ZIF-90 can also be ascribed to such compositional differences between the synthesis solution and the resulting product. It is indicated that OHC-IM is incorporated into the frameworks at higher contents than that of the initial synthesis solution. By using HCOONa, IM linkers will be adequately deprotonated before coordinating with Zn^{2+} to make it more likely to crystallize in a more homogeneous form rather than a random mixture of crystalline phases, which contributes to the competitive coordination of the two linkers with the Zn^{2+} metal center. As a result, the oversaturation of the precursor species is decreased and the nucleation is prolonged.[61] It is probably that the OHC-IM linkers are coordinated with the metal centers more favorably than the 2-MeIM linkers. In general, the observed OHC-IM contents in the resulting ZIF-8-90 frameworks are found to increase monotonically with its increasing dosage in the

Table 2. Chemical Compositions of ZIF-8-90 Samples

sample	chemical composition	*n*(OHC-IM)/(*n*(2-MeIM) + *n*(OHC-IM)) used for synthesis	*n*(OHC-IM)/(*n*(2-MeIM) + *n*(OHC-IM)) observed in product
ZIF-8	$Zn(MeIM)_2$	0.00	0.00
ZIF-8-90-S1	$Zn[(MeIM)_{0.69}(OHC\text{-}IM)_{0.31}]_2$	0.25	0.31
ZIF-8-90-S2	$Zn[(MeIM)_{0.45}(OHC\text{-}IM)_{0.55}]_2$	0.375	0.55
ZIF-8-90-S3	$Zn[(MeIM)_{0.27}(OHC\text{-}IM)_{0.73}]_2$	0.5	0.73
ZIF-8-90-S4	$Zn[(MeIM)_{0.18}(OHC\text{-}IM)_{0.82}]_2$	0.625	0.82
ZIF-8-90-S5	$Zn[(MeIM)_{0.12}(OHC\text{-}IM)_{0.88}]_2$	0.75	0.88
ZIF-90	$Zn(OHC\text{-}IM)_2$	1.00	1.00

DOI: 10.1021/acs.iecr.9b00941
Ind. Eng. Chem. Res. 2019, 58, 13274−13283

original synthesis solutions. It is confirmed that the linker compositions of hybrid ZIF-8-90 can be consecutively tuned by altering the ligand proportions in synthesis systems and, therefore, expected to provide well-controlled structures and performances.

3.2. SEM and XRD Analyses. The SEM images of ZIF samples with different ligand compositions are presented in Figure S3. All ZIF samples show a typical crystal morphology of rhombic dodecahedron and a crystal size of 5−10 μm. For ZIF-8-90 samples, the crystal size decreases slightly with an increasing OHC-IM to 2-MeIM ratio.

To confirm the crystalline phase compositions, the powder XRD analyses were conducted on the synthesized samples (see Figure 3). Meanwhile, we also used the Reflex module of the

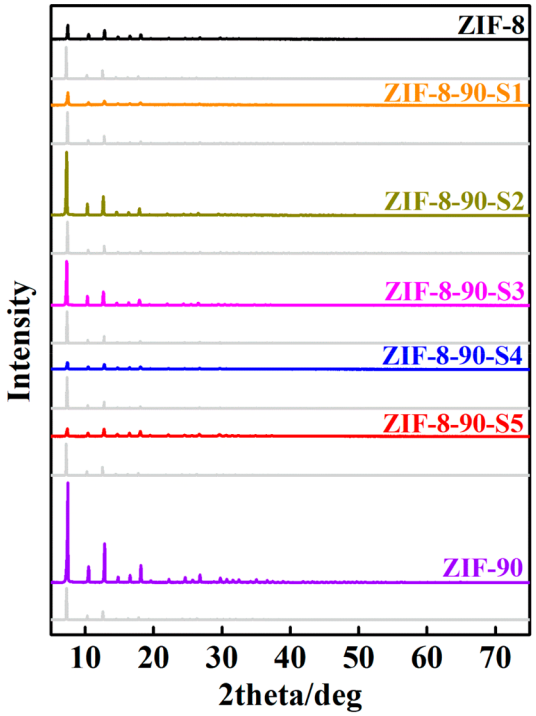

Figure 3. X-ray diffraction patterns of different samples. (The gray curves represent the simulated results.)

Materials Studio Package to simulate the X-ray diffraction patterns of different ZIF samples. From the XRD results, the hybrid ZIF-8-90 samples show essentially identical XRD patterns to that of single-linker ZIF-8 and ZIF-90 structures and all samples have identical $I\bar{4}3m$ cubic unit cells without any other impurity phases. Furthermore, our current XRD details indicate that all samples have the same framework topology and only small differences in electron density and lattice constant, which is in agreement with previously reported results.[43]

3.3. TG-DSC Analyses. TG-DSC analyses were employed here to reveal the structural evolution on heating and evaluate the thermal stability of different ZIF-8-90 samples. From the TG curves, two-stage mass loss events can be recognized (see Figure 4). The first event in the low-temperature region (lower than 300 °C) corresponds to the release of guest species such as adsorbed water and residual solvent in synthetic products. The second TG event, lasting from around 300 °C to around 600 °C, is associated with the decomposition of the ZIF-8-90 structure. As the proportion of OHC-IM linker in the ZIF-8-90

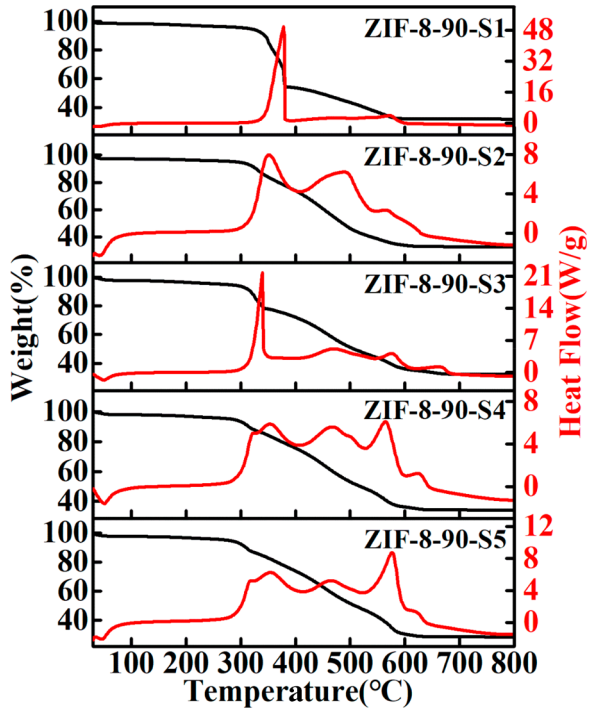

Figure 4. TG-DSC profiles of different samples.

framework increases, the collapsing temperature of the hybrid framework keeps decreasing. DSC peaks are centered at 372 °C for ZIF-8-90-S1, 331 °C for ZIF-8-90-S2, 324 °C for ZIF-8-90-S3, 311 °C for ZIF-8-90-S4, and 308 °C for ZIF-8-90-S5. Thompson et al.[45] have reported that the ZIF-90 structure starts to decompose at a much lower temperature as compared to the ZIF-8 architecture. This can be attributed to typically higher oxidation activity of the aldehyde group under exposure to air at elevated temperatures. When the temperature rises to higher than 700 °C, the mass of each sample will reach a plateau, accounting for 31.85−34.08% mass of the initial sample. Assuming that ZIF-8-90 structure is completely transformed to zinc oxide (with the elements C, H, and O escaping in forms of CO_2 and vaporized H_2O), theoretically the remaining mass fraction, on a stoichiometric basis, should be in the range of 34.44% (ZIF-8-90-S1) to 32.26% (ZIF-8-90-S5), which is in good agreement with the experimentally observed results.

3.4. Effect of Tuned Ligand Compositions on Pore Structures of ZIF-8-90. To further explore the impacts of the mixed linkers introduced to the ZIF frameworks on pore structures, N_2 adsorption on all synthesized samples were measured (see Figure 5 for N_2 adsorption isotherms). Pore structure parameters calculated from N_2 adsorption isotherms are summarized in Table 3. The inclusion of OHC-IM ligand in ZIF-8-90 structures reduces both the BET specific surface area and the pore volume of the ligand-combined samples. With the exchange of 2-MeIM with OHC-IM, two hydrogen atoms are replaced by one oxygen atom, and this structural feature makes the effective void inside ZIF-90 structure smaller than that of ZIF-8. Therefore, the pore volume of ZIF-8-90 decreases with an increasing OHC-IM to 2-MeIM molar ratio. It has been shown that ZIF-90 exerts hysteresis at $P/P_0 \sim 0.42$, which is attributed to a constriction in the micropores.[62] As for ZIF-90 and all ZIF-8-90 samples, there are two inflection points in N_2 adsorption isotherms. The first one at lower

DOI: 10.1021/acs.iecr.9b00941
Ind. Eng. Chem. Res. 2019, 58, 13274−13283

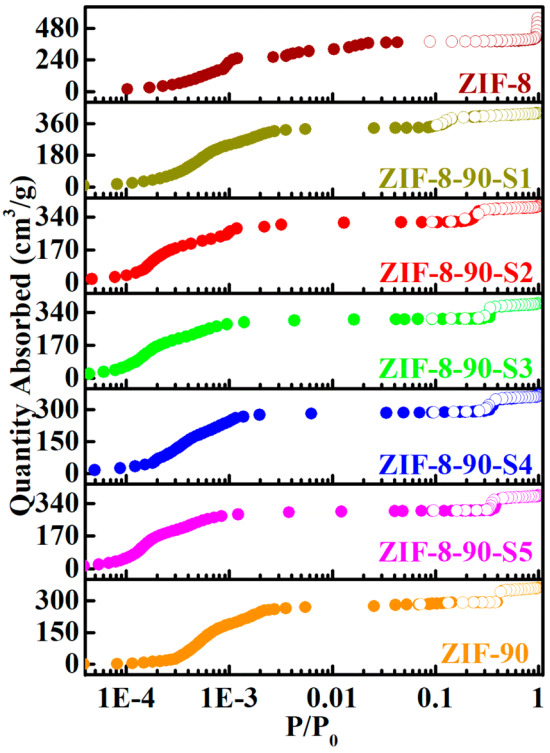

Figure 5. N_2 adsorption isotherms of different samples. (The solid points represent the adsorption data and the hollow points represent the desorption data.).

Table 3. Pore Structure Analyses of ZIF-8-90 Samples

sample	S_{BET}[a] (m^2 g^{-1})	V_p[b] (cm^3 g^{-1})
ZIF-8	1532	0.856
ZIF-8-90-S1	1374	0.649
ZIF-8-90-S2	1276	0.613
ZIF-8-90-S3	1210	0.600
ZIF-8-90-S4	1192	0.566
ZIF-8-90-S5	1208	0.596
ZIF-90	1075	0.486

[a]S_{BET}, BET specific surface area. [b]V_p, pore volume.

relative pressure (e.g., P/P_0 of around 2×10^{-4}) is assigned to the gate-opening effect, and the second one can be attributed to constriction of the micropores at higher relative pressure (e.g., P/P_0 of around 0.35) resulting from the aldehyde functionality on the OHC-IM ligands.[63] As the OHC-IM proportion in the hybrid framework increases, the second inflection shifts to higher relative pressure (changing from $P/P_0 = 0.12$ for ZIF-8-90-S1 to $P/P_0 = 0.38$ for ZIF-8-90-S5). As for the isotherms of the ZIF-8 sample, the second inflection disappears due to the absence of an aldehyde group in the ZIF-8 structure. It can be explained that the hybrid ZIF-8-90 structures are constructed by the controllable assembly of 2-MeIM and OHC-IM linkers into the topology frameworks. As a result, the consecutively evolved framework structures can be achieved and, therefore, can be expected to provide the well-designed pore dimension. In addition, the micropore and mesopore size distributions for the ZIF-8-90 samples were calculated by using the H−K and BJH methods, respectively (see Figure 6). As it can be expected, the pore size changes with an increase of OHC-IM proportion in the framework. Specifically, the mesopore width monotonically increases from

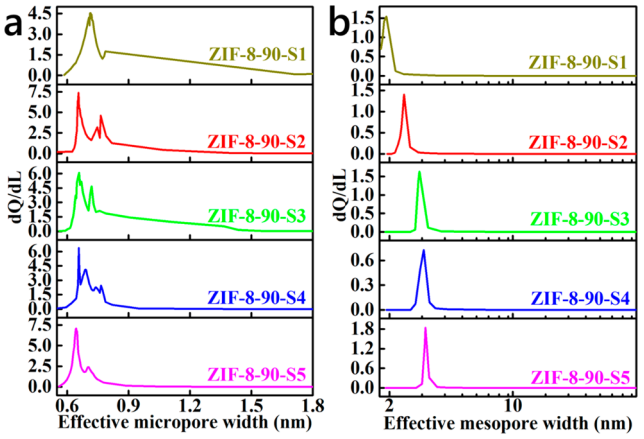

Figure 6. (a) Micropore and (b) mesopore size distributions of different samples.

2.18 to 3.29 nm as the OHC-IM proportion increases from 0.31 (ZIF-8-90-S1) to 0.88 (ZIF-8-90-S5). Correspondingly, the average micropore diameter is reduced from 0.72 nm for ZIF-8−90-S1 to 0.65 nm for ZIF-8-90-S5. Such characteristics of pore structure can be attributed to the well-defined frameworks involving tuned organic ligand compositions. Moreover, the samples of ZIF-8-90-S2, ZIF-8-90-S3, and ZIF-8-90-S4 show wider micropore size distributions as compared to the ZIF-8-90-S1 and ZIF-8-90-S5 samples. Table 4 demonstrates the assemble possibilities for the six-membered ring of ZIF-8-90 frameworks with different ligand compositions. When the OHC-IM ratio is either very low (i.e., OHC-IM to 2-MeIM ratio of 1:5) or very high (i.e., OHC-IM to 2-MeIM ratio of 5:1), the two organic ligands contained in the frameworks can be arranged in only one way. By contrast, the OHC-IM and 2-MeIM ligands can be assembled into the frameworks in three ways when the ratio has a medium value of 2:4, 3:3, or 4:2. Considering an actual crystallization process, the ligands are linked to other species not always strictly according to the stoichiometric rule. Hence, various arrangements of ligands can happen in the synthesis of the ZIF-8-90 framework. There are six IM groups in one six-membered ring of the cubic unit cell of the ZIF-8-90 framework. Assuming that the substituents on each group are random (see Figure 7), there are 11 possible six-membered ring structures that can be formed (see Table 4) for each synthesis case. It is reasonable that different ZIF-8-90 samples have distinct micropore size distributions. As a result, the expected evolution of micropore structure is confirmed by present pore size analysis results.

3.5. Effect of Tuned Ligand Compositions on *n*-Hexane Adsorption. To evaluate the adsorption ability of *n*-hexane on ZIF-8-90, gas adsorption isotherms were measured first (see Figure 8). Furthermore, the experimental data were correlated using the Langmuir−Freundlich model expressed as eq 2.

$$q_e = q_{max} \frac{(bP_e)^N}{1 + (bP_e)^N} \quad (2)$$

where b and N are the L−F constants, respectively. q_{max} is the maximum adsorption amount (mg *n*-hexane per g adsorbent), and q_e refers to the equilibrated adsorption amount (mg/g) under partial pressure of P_e (Pa).

In addition, a dimensionless constant that is defined as the separation factor (R_L) was used to evaluate the relative

DOI: 10.1021/acs.iecr.9b00941
Ind. Eng. Chem. Res. 2019, 58, 13274−13283

Table 4. Assemble Possibilities for Six-Membered Ring of ZIF-8-90 Frameworks with Different Ligand Compositions[a]

OHC-IM to 2-MeIM ratio	Arrangement mode of ligands
1:5	
2:4	
3:3	
4:2	
5:1	

[a]The blue and yellow sticks represent 2-MeIM and OHC-IM ligands, respectively.

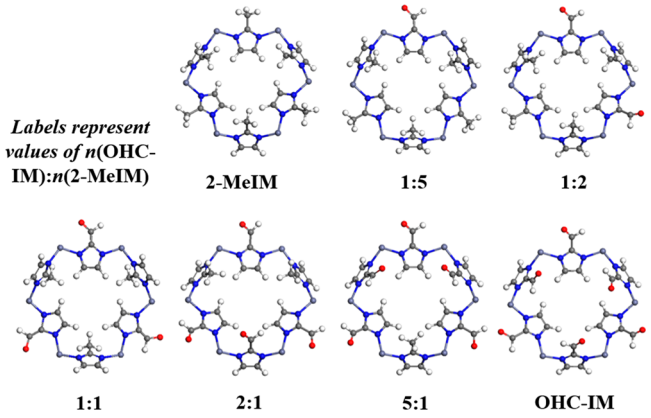

Figure 7. Simulated structures of single-linker and mixed-linker ZIFs.

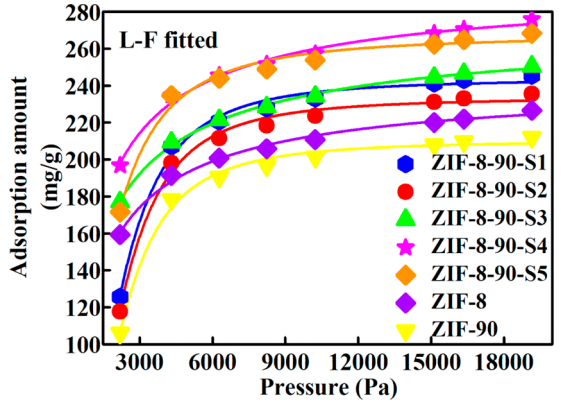

Figure 8. Gas adsorption isotherms of *n*-hexane on different samples at 298 K.

adsorption performance of *n*-hexane on different ZIF samples and could be calculated using eq 3.

$$R_L = \frac{1}{1 + bP_0} \tag{3}$$

where P_0 represents the initial pressure of adsorbate in the adsorption system (Pa). R_L represents the nature of adsorption: unfavorable ($R_L > 1$), linear ($R_L = 1$), favorable ($0 < R_L < 1$) or irreversible ($R_L = 0$).[64] A lower R_L value suggests more favorable adsorption.

The fitted results by applying L−F model are summarized in Table 5. The ZIF-8-90-S4 sample shows the largest q_{max} and the smallest R_L, indicating that the most favorable adsorption affinity to *n*-hexane is found on the ZIF-8-90-S4 sample with a medium OHC-IM to 2-MeIM molar ratio. Such results suggest that the resulting ZIF-8-90 samples are mainly composed of a mixed-linker of OHC-IM and 2-MeIM.

We also conducted the batch liquid adsorption tests at 298 K to evaluate the *n*-hexane uptakes of different ZIF-8-90 samples from a liquid mixture of *n*-hexane/cyclohexane. Again,

DOI: 10.1021/acs.iecr.9b00941
Ind. Eng. Chem. Res. 2019, 58, 13274−13283

Table 5. L−F Model Parameters for *n*-Hexane Adsorption on ZIF-8-90 Samples at 298 K

sample	q_{max}, mg g^{-1}	b^a	N^a	$R_L{}^b$	R^{2c}
ZIF-8-90-S1	243	4.72×10^{-4}	2.21	0.49	0.99
ZIF-8-90-S2	233	4.63×10^{-4}	2.26	0.49	0.99
ZIF-8-90-S3	275	9.92×10^{-4}	0.77	0.31	0.99
ZIF-8-90-S4	295	1.07×10^{-3}	0.83	0.30	0.99
ZIF-8-90-S5	267	6.37×10^{-4}	1.73	0.42	0.98
ZIF-8	243	3.04×10^{-4}	0.86	0.60	0.99
ZIF-90	210	4.25×10^{-4}	1.89	0.52	0.99

[a] *b*, *N*, L−F constants. [b] R_L represents the nature of adsorption. [c] R^2, correlation coefficient.

we found the highest *n*-hexane adsorption capacity on the ZIF-8-90-S4 sample (see Figure 9 for the experimental results).

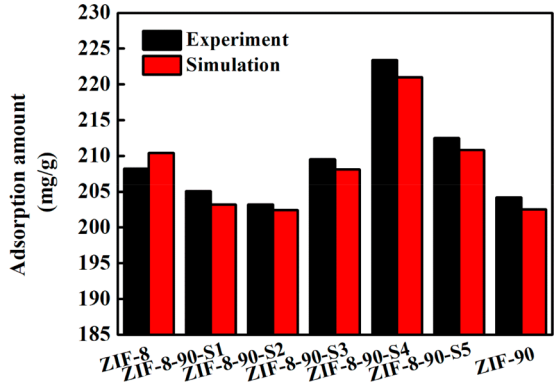

Figure 9. Experimental and simulated *n*-hexane adsorption capacities on different samples.

The GCMC simulation results also support our experimental findings by exhibiting the consistent fluctuation with experimental adsorption amounts when changing ligand compositions of ZIF samples (see the same figure for the simulation results). These findings are in good agreement with the aforementioned gas adsorption results (see Table 5 for q_{max}).

Additionally, computational simulation was carried out to reveal the van der Waals interaction energy involved in *n*-hexane adsorption on different ZIF samples. In order to exclude the intermolecular force, the adsorption was strictly restricted with only one molecule confined in each cage when we used the Locate Task in the Sorption module of the Accelrys Package to calculate the changes of the van der Waals interaction energy (see Figure S2). The individually calculated energy is presented in Figure 10. It can be seen from the simulation results that the van der Waals interaction energy reaches a peak value of 5.508 kcal/mol at an OHC-IM proportion of 0.792 (OHC-IM to 2-MeIM ratio of 19:5) (very close to the observed value of ZIF-8-90-S4), which corresponds to the results of aforementioned batch liquid adsorption test, gas adsorption measurement, and computational adsorption simulation. Since the ZIF-8 framework has weaker polarity than ZIF-90,[45] all ZIF-8-90 retain the same topological structure of ZIF-8. As a result, once the aldehyde group is incorporated into the framework, the heterogeneity of the framework charge distribution is increased and the resulting hybrid ZIF-8-90 materials will have stronger polarity than ZIF-8 and larger pore volume than ZIF-90. The increase

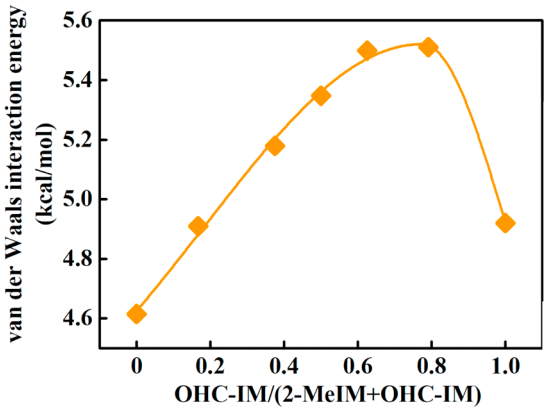

Figure 10. Calculated van der Waals interaction energy involved in *n*-hexane adsorption on different ZIF-8-90 structures.

in polarity contributes to the strengthened guest−host van der Waals interaction resulting from the enhanced induction force between nonpolar alkane molecule and the defined framework and therefore energetically exerts a positive effect on the adsorption of *n*-hexane on hybrid ZIF-8-90 structures.

4. CONCLUSIONS

In summary, we have demonstrated a series of mixed-linker ZIF-8-90 structures, which can be promising porous structures for *n*-hexane from various hydrocarbon mixtures after fine manipulation of structure and activity. The hybrid ZIF-8-90 samples were synthesized by using the OHC-IM and 2-MeIM ligands simultaneously. All samples were characterized, and the structural evolution was explored through applying various analysis techniques including FESEM, Raman, XRD, TG-DSC, N_2 adsorption, and ^{1}H NMR analyses. Well-designed ligand compositions of ZIF structures contribute to the continuously switchable pore structure as well as framework polarity. Consequently, the tunable adsorption affinity to *n*-hexane probe are confirmed by adsorption measurements coupled with GCMC simulation. Such compositional and structural evolution along with organic ligand exchange benefits the adsorption performance for *n*-hexane. The present study highlights the tunability of adsorption properties from energetics prospective and provides insights into the underlying implications for the function-enhanced tuning of MOF architectures.

■ ASSOCIATED CONTENT

Supporting Information

The Supporting Information is available free of charge on the ACS Publications website at DOI: 10.1021/acs.iecr.9b00941.

^{1}H NMR spectra for different ZIF-8-90 samples, simulated adsorption of one molecule into each cage of ZIF frameworks, and SEM images of ZIFs (PDF)

■ AUTHOR INFORMATION

Corresponding Author

*E-mail: sunhui@ecust.edu.cn.

ORCID

Hui Sun: 0000-0002-8544-756X

Di Wu: 0000-0001-6879-321X

Notes

The authors declare no competing financial interest.

DOI: 10.1021/acs.iecr.9b00941
Ind. Eng. Chem. Res. 2019, 58, 13274−13283

■ ACKNOWLEDGMENTS

This work is financially supported by the National Natural Science Foundation of China (Grants 91634112 and 21878097), the Natural Science Foundation of Shanghai (Grant 16ZR1408100), and the Open Project of State Key Laboratory of Chemical Engineering (Grant SKL-ChE-16C01). D.W. acknowledges the institutional funds from the Gene and Linda Voiland School of Chemical Engineering and Bioengineering at Washington State University.

■ ABBREVIATIONS

2-MeIM = 2-methylimidazole
OHC-IM = carboxaldehyde-2-imidazole
MeOH = methanol
FESEM = field emission scanning electron microscopy
EDS = energy-dispersive spectrometer
XRD = X-ray diffraction
TG-DSC = thermogravimetry and differential scanning calorimetry
BET = Brunauer−Emmet−Teller
H−K = Harvath−Kawazoe
BJH = Barrett−Joyner−Halenda
^{1}H NMR = ^{1}H nuclear magnetic resonance
GCMC = Grand Canonical Monte Carlo

■ REFERENCES

(1) Zhang, L.; Qian, G.; Liu, Z.; Cui, Q.; Wang, H.; Yao, H. Adsorption and separation properties of n-pentane/isopentane on ZIF-8. *Sep. Purif. Technol.* **2015**, *156*, 472.
(2) Bohme, U.; Barth, B.; Paula, C.; Kuhnt, A.; Schwieger, W.; Mundstock, A.; Caro, J.; Hartmann, M. Ethene/ethane and propene/propane separation via the olefin and paraffin selective metal-organic framework adsorbents CPO-27 and ZIF-8. *Langmuir* **2013**, *29* (27), 8592.
(3) Rubes, M.; Wiersum, A. D.; Llewellyn, P. L.; Grajciar, L.; Bludsky, O.; Nachtigall, P. Adsorption of propane and propylene on CuBTC metal-organic framework: combined theoretical and experimental investigation. *J. Phys. Chem. C* **2013**, *117* (21), 11159.
(4) Larriba, M.; Navarro, P.; González, E. J.; García, J.; Rodríguez, F. Separation of BTEX from a naphtha feed to ethylene crackers using a binary mixture of [4empy][Tf_2N] and [emim][DCA] ionic liquids. *Sep. Purif. Technol.* **2015**, *144*, 54.
(5) Marker, T. L.; Petri, J. A.; Luebke, C. P.; Kalnes, T. N.; McCall, M. J. *Use of n-paraffin adsorption to increase selectivity and yield of synthetic distillate fuel*. U.S. Patent Application 20140005450 A1, January 2, 2014.
(6) Chekantsev, N. V.; Gyngazova, M. S.; Ivanchina, E. D. Mathematical modeling of light naphtha (C5, C6) isomerization process. *Chem. Eng. J.* **2014**, *238*, 120.
(7) Bury, W.; Walczak, A. M.; Leszczyński, M. K.; Navarro, J. A. Rational Design of Noncovalent Diamondoid Microporous Materials for Low-Energy Separation of C6-Hydrocarbons. *J. Am. Chem. Soc.* **2018**, *140* (44), 15031.
(8) Espada, J. J.; Coutinho, J. A.; Pena, J. L. Evaluation of methods for the extraction and characterization of waxes from crude oils. *Energy Fuels* **2010**, *24* (3), 1837.
(9) Wijesekera, K. N.; Adams, T. A. Semicontinuous distillation of quintenary and N-ary mixtures. *Ind. Eng. Chem. Res.* **2015**, *54* (51), 12877.
(10) Kwon, H. T.; Jeong, H. K. Improving propylene/propane separation performance of zeolitic-imidazolate framework ZIF-8 membranes. *Chem. Eng. Sci.* **2015**, *124*, 20.
(11) Venna, S. R.; Carreon, M. A. Metal organic framework membranes for carbon dioxide separation. *Chem. Eng. Sci.* **2015**, *124*, 3.
(12) Kumar, S.; Singh, A.; Sinha, P. K.; Kamachi Mudali, U.; Natarajan, R. Development of a urea-adduct process for recovery of n-alkane based diluent from spent PUREX/UREX solvent. *J. Radioanal. Nucl. Chem.* **2012**, *293*, 721.
(13) Zhang, Z.; Xian, S.; Xia, Q.; Wang, H.; Li, Z.; Li, J. Enhancement of CO2 adsorption and CO2/N2 selectivity on ZIF-8 via postsynthetic modification. *AIChE J.* **2013**, *59* (6), 2195.
(14) Santos, J. C.; Cruz, P.; Regala, T.; Magalhaes, F. D.; Mendes, A. High-purity oxygen production by pressure swing adsorption. *Ind. Eng. Chem. Res.* **2007**, *46* (2), 591.
(15) Krishna, R.; Van Baten, J. M. Diffusion of hydrocarbon mixtures in MFI zeolite: Influence of intersection blocking. *Chem. Eng. J.* **2008**, *140* (1−3), 614.
(16) Wahby, A.; Ramos-Fernández, J. M.; Martínez-Escandell, M.; Sepúlveda-Escribano, A.; Silvestre-Albero, J.; Rodríguez-Reinoso, F. High-surface-area carbon molecular sieves for selective CO_2 adsorption. *ChemSusChem* **2010**, *3* (8), 974.
(17) Serrano, D. P.; Calleja, G.; Botas, J. A.; Gutierrez, F. J. Characterization of adsorptive and hydrophobic properties of silicalite-1, ZSM-5, TS-1 and Beta zeolites by TPD techniques. *Sep. Purif. Technol.* **2007**, *54* (1), 1.
(18) Li, J. R.; Sculley, J.; Zhou, H. C. Metal-organic frameworks for separations. *Chem. Rev.* **2012**, *112* (2), 869.
(19) Herm, Z. R.; Bloch, E. D.; Long, J. R. Hydrocarbon separations in metal-organic frameworks. *Chem. Mater.* **2014**, *26* (1), 323.
(20) Bozbiyik, B.; Duerinck, T.; Lannoeye, J.; De Vos, D. E.; Baron, G. V.; Denayer, J. F. Adsorption and separation of n-hexane and cyclohexane on the UiO-66 metal-organic framework. *Microporous Mesoporous Mater.* **2014**, *183*, 143.
(21) Patel, H. A.; Hyun Je, S.; Park, J.; Chen, D. P.; Jung, Y.; Yavuz, C. T.; Coskun, A. Unprecedented high-temperature CO_2 selectivity in N_2-phobic nanoporous covalent organic polymers. *Nat. Commun.* **2013**, *4*, 1357.
(22) Yuan, D.; Lu, W.; Zhao, D.; Zhou, H. C. Highly stable porous polymer networks with exceptionally high gas□uptake capacities. *Adv. Mater.* **2011**, *23* (32), 3723.
(23) Iyer, A.; Del-Pilar, J.; King'ondu, C. K.; Kissel, E.; Garces, H. F.; Huang, H.; El-Sawy, A. M.; Dutta, P. K.; Suib, S. L. Water oxidation catalysis using amorphous manganese oxides, octahedral molecular sieves (OMS-2), and octahedral layered (OL-1) manganese oxide structures. *J. Phys. Chem. C* **2012**, *116* (10), 6474.
(24) Buonsanti, R.; Llordes, A.; Aloni, S.; Helms, B. A.; Milliron, D. J. Tunable infrared absorption and visible transparency of colloidal aluminum-doped zinc oxide nanocrystals. *Nano Lett.* **2011**, *11* (11), 4706.
(25) Kleist, W.; Maciejewski, M.; Baiker, A. MOF-5 based mixed-linker metal-organic frameworks: Synthesis, thermal stability and catalytic application. *Thermochim. Acta* **2010**, *499* (1−2), 71.
(26) Reinsch, H.; Waitschat, S.; Stock, N. Mixed-linker MOFs with CAU-10 structure: synthesis and gas sorption characteristics. *Dalton. T.* **2013**, *42* (14), 4840.
(27) Kobielska, P. A.; Howarth, A. J.; Farha, O. K.; Nayak, S. Metal-organic frameworks for heavy metal removal from water. *Coord. Chem. Rev.* **2018**, *358*, 92.
(28) Lee, D. Y.; Yoon, S. J.; Shrestha, N. K.; Lee, S. H.; Ahn, H.; Han, S. H. Unusual energy storage and charge retention in Co-based metal-organic-frameworks. *Microporous Mesoporous Mater.* **2012**, *153*, 163.
(29) Llabres i Xamena, F.; Casanova, O.; Galiasso Tailleur, R.; Garcia, H.; Corma, A. Metal organic frameworks (MOFs) as catalysts: A combination of Cu^{2+} and Co^{2+} MOFs as an efficient catalyst for tetralin oxidation. *J. Catal.* **2008**, *255* (2), 220.
(30) Stavila, V.; Talin, A. A.; Allendorf, M. D. MOF-based electronic and opto-electronic devices. *Chem. Soc. Rev.* **2014**, *43* (16), 5994.
(31) Meyer, L. V.; Schönfeld, F.; Müller-Buschbaum, K. Lanthanide based tuning of luminescence in MOFs and dense frameworks-from mono-and multimetal systems to sensors and films. *Chem. Commun.* **2014**, *50* (60), 8093.

DOI: 10.1021/acs.iecr.9b00941
Ind. Eng. Chem. Res. 2019, 58, 13274−13283

(32) McKinlay, A. C.; Morris, R. E.; Horcajada, P.; Férey, G.; Gref, R.; Couvreur, P.; Serre, C. BioMOFs: metal-organic frameworks for biological and medical applications. *Angew. Chem., Int. Ed.* **2010**, *49* (36), 6260.
(33) Zhu, M.; Venna, S. R.; Jasinski, J. B.; Carreon, M. A. Room-temperature synthesis of ZIF-8: the coexistence of ZnO nanoneedles. *Chem. Mater.* **2011**, *23* (16), 3590.
(34) Wu, Y.; Zhou, M.; Zhang, B.; Wu, B.; Li, J.; Qiao, J.; Guan, X.; Li, F. Amino acid assisted templating synthesis of hierarchical zeolitic imidazolate framework-8 for efficient arsenate removal. *Nanoscale* **2014**, *6* (2), 1105.
(35) Pan, Y.; Liu, Y.; Zeng, G.; Zhao, L.; Lai, Z. Rapid synthesis of zeolitic imidazolate framework-8 (ZIF-8) nanocrystals in an aqueous system. *Chem. Commun.* **2011**, *47* (7), 2071.
(36) Park, K. S.; Ni, Z.; Côté, A. P.; Choi, J. Y.; Huang, R.; Uribe-Romo, F. J.; Chae, H. K.; O'Keeffe, M.; Yaghi, O. M. Exceptional chemical and thermal stability of zeolitic imidazolate frameworks. *Proc. Natl. Acad. Sci. U. S. A.* **2006**, *103*, 10186.
(37) Banerjee, R.; Phan, A.; Wang, B.; Knobler, C.; Furukawa, H.; O'keeffe, M.; Yaghi, O. M. High-throughput synthesis of zeolitic imidazolate frameworks and application to CO2 capture. *Science* **2008**, *319* (5865), 939.
(38) Phan, A.; Doonan, C. J.; Uribe-Romo, F. J.; Knobler, C. B.; O'keeffe, M.; Yaghi, O. M. Synthesis, structure, and carbon dioxide capture properties of zeolitic imidazolate frameworks. *Acc. Chem. Res.* **2010**, *43* (1), 58.
(39) Zhang, J.; Zhang, T.; Yu, D.; Xiao, K.; Hong, Y. Transition from ZIF-L-Co to ZIF-67: a new insight into the structural evolution of zeolitic imidazolate frameworks (ZIFs) in aqueous systems. *CrystEngComm* **2015**, *17* (43), 8212.
(40) Gücüyener, C.; van den Bergh, J.; Gascon, J.; Kapteijn, F. Ethane/ethene separation turned on its head: selective ethane adsorption on the metal-organic Framework ZIF-7 through a gate-opening mechanism. *J. Am. Chem. Soc.* **2010**, *132* (50), 17704.
(41) Lin, K. Y. A.; Chang, H. A. Efficient adsorptive removal of humic acid from water using zeolitic imidazole framework-8 (ZIF-8). *Water, Air, Soil Pollut.* **2015**, *226* (2), 10.
(42) Mulfort, K. L.; Hupp, J. T. Chemical reduction of metal-organic framework materials as a method to enhance gas uptake and binding. *J. Am. Chem. Soc.* **2007**, *129* (31), 9604.
(43) Eum, K.; Jayachandrababu, K. C.; Rashidi, F.; Zhang, K.; Leisen, J.; Graham, S.; Lively, R. P.; Chance, R. R.; Sholl, D. S.; Jones, C. W.; Nair, S. Highly tunable molecular sieving and adsorption properties of mixed-linker zeolitic imidazolate frameworks. *J. Am. Chem. Soc.* **2015**, *137* (12), 4191.
(44) Gee, J. A.; Chung, J.; Nair, S.; Sholl, D. S. Adsorption and diffusion of small alcohols in zeolitic imidazolate frameworks ZIF-8 and ZIF-90. *J. Phys. Chem. C* **2013**, *117* (6), 3169.
(45) Thompson, J. A.; Blad, C. R.; Brunelli, N. A.; Lydon, M. E.; Lively, R. P.; Jones, C. W.; Nair, S. Hybrid zeolitic imidazolate frameworks: controlling framework porosity and functionality by mixed-linker synthesis. *Chem. Mater.* **2012**, *24* (10), 1930.
(46) Accelrys. *Materials Studio, Modeling Getting Started*; Accelrys Software Inc.: San Diego, CA, 2004.
(47) Zhang, K.; Lively, R. P.; Zhang, C.; Chance, R. R.; Koros, W. J.; Sholl, D. S.; Nair, S. Exploring the Framework Hydrophobicity and Flexibility of ZIF-8: From Biofuel Recovery to Hydrocarbon Separations. *J. Phys. Chem. Lett.* **2013**, *4* (21), 3618.
(48) Morris, W.; Doonan, C. J.; Furukawa, H.; Banerjee, R.; Yaghi, O. M. Crystals as molecules: postsynthesis covalent functionalization of zeolitic imidazolate frameworks. *J. Am. Chem. Soc.* **2008**, *130* (38), 12626.
(49) Otero-De-La-Roza, A.; Johnson, E. R.; Contreras-García, J. Revealing non-covalent interactions in solids: NCI plots revisited. *Phys. Chem. Chem. Phys.* **2012**, *14* (35), 12165.
(50) Xu, Q.; Zhong, C. A general approach for estimating framework charges in metal-organic frameworks. *J. Phys. Chem. C* **2010**, *114* (11), 5035.
(51) Lamia, N.; Jorge, M.; Granato, M. A.; Almeida Paz, F. A.; Chevreau, H.; Rodrigues, A. E. Adsorption of propane, propylene and isobutane on a metal-organic framework: Molecular simulation and experiment. *Chem. Eng. Sci.* **2009**, *64* (14), 3246.
(52) Babarao, R.; Hu, Z.; Jiang, J.; Chempath, S.; Sandler, S. I. Storage and separation of CO_2 and CH_4 in silicalite, C168 schwarzite, and IRMOF-1: a comparative study from Monte Carlo simulation. *Langmuir* **2007**, *23* (2), 659.
(53) Bae, Y.-S.; Mulfort, K. L.; Frost, H.; Ryan, P.; Punnathanam, S.; Broadbelt, L. J.; Hupp, J. T.; Snurr, R. Q. Separation of CO_2 from CH_4 using mixed-ligand metal-organic frameworks. *Langmuir* **2008**, *24* (16), 8592.
(54) Martin, M. G.; Siepmann, J. I. Transferable potentials for phase equilibria. 1. United-atom description of n-alkanes. *J. Phys. Chem. B* **1998**, *102* (14), 2569.
(55) Dubbeldam, D.; Calero, S.; Vlugt, T. J. H.; Krishna, R.; Maesen, T. L.; Smit, B. United atom force field for alkanes in nanoporous materials. *J. Phys. Chem. B* **2004**, *108* (33), 12301.
(56) Wick, C. D.; Martin, M. G.; Siepmann, J. I. Transferable potentials for phase equilibria. 4. United-atom description of linear and branched alkenes and alkylbenzenes. *J. Phys. Chem. B* **2000**, *104* (33), 8008.
(57) Granato, M. A.; Vlugt, T. J.; Rodrigues, A. E. Molecular simulation of propane- propylene binary adsorption equilibrium in zeolite 13X. *Ind. Eng. Chem. Res.* **2007**, *46* (22), 7239.
(58) Mayo, S. L.; Olafson, B. D.; Goddard, W. A. DREIDING: a generic force field for molecular simulations. *J. Phys. Chem.* **1990**, *94* (26), 8897.
(59) Düren, T.; Sarkisov, L.; Yaghi, O. M.; Snurr, R. Q. Design of new materials for methane storage. *Langmuir* **2004**, *20* (7), 2683.
(60) Tammer, M. Infrared and Raman characteristic group frequencies: tables and charts. *Colloid Polym. Sci.* **2004**, *283*, 235.
(61) Diring, S.; Furukawa, S.; Takashima, Y.; Tsuruoka, T.; Kitagawa, S. Controlled multiscale synthesis of porous coordination polymer in nano/micro regimes. *Chem. Mater.* **2010**, *22* (16), 4531.
(62) Stavitski, E.; Pidko, E. A.; Couck, S.; Remy, T.; Hensen, E. J. M.; Weckhuysen, B. M.; Denayer, J.; Gascon, J.; Kapteijn, F. Complexity behind CO_2 capture on NH_2-MIL-53 (Al). *Langmuir* **2011**, *27* (7), 3970.
(63) Morris, W.; Doonan, C. J.; Furukawa, H.; Banerjee, R.; Yaghi, O. M. Crystals as molecules: postsynthesis covalent functionalization of zeolitic imidazolate frameworks. *J. Am. Chem. Soc.* **2008**, *130* (38), 12626.
(64) Weber, T. W.; Chakravorti, R. K. Pore and solid diffusion models for fixed-bed adsorbers. *AIChE J.* **1974**, *20* (2), 228.

DOI: 10.1021/acs.iecr.9b00941
Ind. Eng. Chem. Res. 2019, 58, 13274−13283